The Binding Site of Sodium in the Gramicidin A Channel: Comparison of Molecular Dynamics with Solid-State NMR Data

Thomas B. Woolf and Benoît Roux
Membrane Transport Research Group, Departments of Physics and Chemistry, Université de Montréal, C.P. 6128, succ. Centre-Ville, Montréal, Québec H3C 3J7 Canada

ABSTRACT The location of the main binding site for sodium in the gramicidin A (GA) channel was investigated with molecular dynamics simulations, using an atomic model of the channel embedded in a fully hydrated dimyristoyl phosphatidycholine (DMPC) bilayer. Twenty-four separate simulations in which a sodium was restrained at different locations along the channel axis were generated. The results are compared with carbonyl ^{13}C chemical shift anisotropy solid-state NMR experimental data previously obtained with oriented GA:DMPC samples. Predictions are made for other solid-state NMR properties that could be observed experimentally. The combined information from experiment and simulation strongly suggests that the main binding sites for sodium are near the channel's mouth, approximately 9.2 Å from the center of the dimer channel. The ^{13}C chemical shift anisotropy of Leu^{10} is the most affected by the presence of a sodium ion in the binding site. In the binding site, the sodium ion is lying off-axis, making contact with two carbonyl oxygens and two single-file water molecules. The main channel ligand is provided by the carbonyl group of the Leu^{10}-Trp^{11} peptide linkage, which exhibits the largest deviation from the ion-free channel structure. Transient contacts with the carbonyl group of Val^{8} and Trp^{15} are also present. The influence of the tryptophan side chains on the channel conductance is examined based on the current information about the binding site.

INTRODUCTION

Detailed information about energetically favorable binding sites along the pathway of a permeating ion is essential to understanding the function of a transmembrane ion channel at the molecular level. Analysis of ion flux data suggests that Na and Ca channels possess a single narrow site, the selectivity filter, through which the permeating ion must pass (Hille, 1992). In contrast, it is generally assumed that K channels function as multiion single-file pores (Hille and Schwarz, 1978; Hille, 1992); the Ca-activated K channel may bind four potassium ions simultaneously, and the delayed rectifier K channel at least three. A characterization of the ligand structure involved in stabilizing an ion along the permeation pathway would be required to understand the selectivity and the transport properties of those biological channels. However, because of the lack of detailed structural information, such questions cannot be addressed at the present time. It is possible to further our understanding of the fundamental aspects of the permeation process by studying simpler pore-forming model systems such as the gramicidin A (GA) channel. One outstanding advantage of the GA channel is the large amount of structural and functional information that is currently available (for a review see Andersen and Koeppe, 1992).

Measurements of the ionic current as a function of an applied transmembrane voltage provide some information about the general location of the rate-determining kinetic processes along the permeation pathway (Hille, 1992). It is observed experimentally that the current-voltage relation is supralinear (less than ohmic), strongly suggesting that the rate-limiting kinetic process opposing the passage of ions through the GA channel occurs in a region that is not very sensitive to the applied transmembrane electric field (Eisenman and Horn, 1983; O. S. Andersen, personal communication). The interpretation relies on an analysis of the data in terms of Eyring rate theory models under the assumption that the transition hopping rates have a simple Arrhenius dependence on the applied voltage (Läuger, 1973). The estimates for the position of the binding site are first obtained in terms of the fraction of the applied transmembrane potential, which is then converted into a position by assuming that the membrane field is constant over the full length of the pore. Based on the flux data, several researchers have concluded that the main binding site is located near the entrance of the channel: Andersen and Procopio (1980) found that the binding site for Na^+ is 14% from the channel entry; Eisenman and Sandblom (1983) estimated the distance from the mouth of the channel to the peak of the entry barrier at 6%; Busath and Szabo (1988) reported that the binding site position for K^+ is 15.4% from the channel entry; and Becker et al. (1992) found that the binding site position is 14% along the way into the channel (probably the most accurate estimate with this method). Assuming a channel length of 25 Å, a fractional distance of 14% corresponds to a binding site position at 9 Å from the center

Received for publication 25 September 1996 and in final form 14 February 1997.

Address reprint requests to Dr. Benoît Roux, Membrane Transport Research Group, Departments of Physics and Chemistry, Université de Montréal, C.P. 6128, succ. Centre-Ville, Montréal, Québec H3C 3J7, Canada. Tel.: 514-343-7105; Fax: 514-343-7586; E-mail: rouxb@plgcn.umontreal.ca.

Dr. Woolf's present address is Departments of Physiology and Biophysics, Johns Hopkins University School of Medicine, 725 N. Wolfe St., Baltimore, MD 21205.

0006-3495/97/05/1930/16 $2.00

of the dimer. Although the conclusion is fairly indirect, it seems unlikely that an ion-binding site could be located deep inside the channel, according to the ion-flux measurements.

The first direct structural evidence of a binding site was obtained using NMR spectroscopy with ^{13}C-labeled GA incorporated in L-α-lysophosphatidylcholine (LPC) lipid vesicles (Urry et al., 1982a,b, 1983). The changes in chemical shift induced by the presence of sodium observed for the carbonyl carbon of Trp^{11} and Trp^{13} indicated that the binding sites are located near the C-terminus of the monomers. Unfortunately, a simple structural interpretation of the observed isotropic ^{13}C backbone carbonyl chemical shifts of GA incorporated into LPC lipid vesicles is difficult because of the high sensitivity of the shielding factor to the local electronic structure. In fact, simple structural interpretations of the chemical shifts can be quite misleading. For example, it was concluded initially on the basis of the ^{13}C chemical shifts that the channel was formed by the association of two left-handed β-helical monomers (Urry et al., 1982b), whereas it was shown later, by two-dimensional NMR of GA incorporated in sodium dodecyl sulfate detergent micelles (Arseniev et al., 1985), that the monomers were in a right-handed helical conformation. Further studies of sodium binding to GA incorporated in LPC vesicles indicated that the main ^{13}C chemical shift change is observed for the carbonyl group of Trp^{11} and Trp^{13} (Jing et al., 1995). A tight and a weak binding constant, presumably corresponding to singly and doubly sodium occupied channels, were estimated to be 67 M^{-1} and 1.7 M^{-1}, respectively (Jing et al., 1995).

The binding of the sodium ion to the GA channel incorporated into oriented dimyristoyl phosphatidylcholine (DMPC) multilayers has been investigated by using solid-state NMR (Smith et al., 1990; Separovic et al., 1994; F. Separovic, personal communication). The measurements determined the change, due to the presence of sodium, in the ^{13}C chemical shift anisotropy (CSA) at specific GA backbone carbonyl sites. The observations indicated that the CSAs of Leu^{10}, Leu^{12}, and Leu^{14} were affected by the presence of sodium, whereas those of Trp^{11} and Trp^{13}, as well as more internal sites, were not. Investigations of similar chemical shifts and dipolar coupling measurements for the ^{15}N-labeled backbone sites are also in progress (T. A. Cross, personal communication). More information about the location of the cation-binding site is also provided by low-angle x-ray scattering on GA incorporated into oriented dilauroylphosphatidylcholine bilayers (Olah et al., 1991). Analysis of the data showed that the binding site for Tl^+ is at 9.6 $\pm$ 0.3 Å from the center of the dimer channel. Although the binding of common ions could not be observed by low-angle x-ray scattering because of their poor scattering contrast, it is likely, from these measurements, that a cationic binding site is located around 9–10 Å. Results from previous molecular dynamics simulations based on an atomic model of the dimer channel embedded in a simplified membrane (Roux and Karplus, 1993) are in qualitative accord with the available experimental data; the calculated free-energy profile of a single Na^+ ion along the axis of the channel exhibited a deep minimum located at each extremity of the dimer corresponding to a cation-binding site; the calculated binding site is located 9.3 Å from the center of the channel, where the Na^+ is in close contact with the carbonyl of Leu^{10}.

In the absence of a high-resolution structure from x-ray crystallography, solid-state NMR experiments provide the most direct information on the detailed structure of the sodium-binding site in the GA channel. To interpret the available data in terms of the three-dimensional structure, it is usually assumed that the observed CSA is dominated by the reorientation of the peptide linkages with respect to the magnetic field (Cross and Opella, 1985); i.e., a small change in the CSA is indicative of a slight distortion of the channel backbone structure due to the presence of an ion in the binding site. Because of the time scale of solid-state NMR, the measured CSA results from an average over rapidly fluctuating sodium positions in fast exchange. A direct structural interpretation of the solid-state NMR data is thus not straightforward. To understand the CSA it is necessary to consider a dynamic average of the CSA over a large number of configurations (Woolf and Roux, 1994).

Although the available experimental data clearly indicate the existence of a cation-binding site located near the entrance of the channel, a detailed structural interpretation is not easily obtained. The goal of the present paper is to use molecular dynamics simulations of a detailed atomic model of the GA channel in a fully hydrated DMPC bilayer to help interpret the available solid-state NMR data concerning the location of the sodium-binding site. In previous publications, the results from the simulation of a similar atomic model were extensively compared to available structural data from solid-state NMR (Woolf and Roux, 1994, 1996). The excellent agreement that was observed with available experimental data strongly supports the validity of the current simulations. In the present study, 24 separate simulations in which a sodium ion was constrained at different locations along the channel axis were generated and analyzed. Analysis of the results shows that the solid-state NMR data are consistent with a major binding site for a sodium ion 9.2 Å from the center of the dimer near the entrance of the channel. The analysis reveals the importance of a dynamic averaging of the ion position in the observed NMR signal and provides insight into the limitations of current atomic models.

METHODOLOGY

Microscopic model

The simulation system represents a model for the oriented samples studied in solid-state NMR experiments (Ketchem et al., 1993; Koeppe et al., 1994; Prosser et al., 1991; Smith et al., 1989). In the experimental systems, the ratio of DMPC:GA is 8:1, and 45% (w/w) water is used. In the atomic model, this corresponds to one GA dimer, 16 DMPC

molecules, and about 700 water molecules. The simulation system consists of a total of 4385 atoms. The three-dimensional structure of the GA channel determined from two-dimensional NMR in sodium dodecyl sulfate detergent micelles was used as a starting point for the calculations (Arseniev et al., 1985). In the simulation system, the center of the bilayer membrane was located at $z = 0$; the channel axis was oriented along the z direction. Hexagonal periodic boundary conditions were applied in the x and y directions to simulate an infinite system within the plane of the bilayer. Periodic images were applied along the z direction to simulate a multilayer system. A translational distance of 60 Å was used along the z axis, and an edge length of 17.2 Å was used for the hexagonal simulation cell, corresponding to a cross-sectional area of 764 Å^2. The recently developed all-hydrogen force field of CHARMM (Brooks et al., 1983), PARAM version 22, for proteins (MacKerell et al., 1992) and lipid molecules (Schlenkrich et al., 1996) was used for all calculations. The TIP3P water potential was used (Jorgensen et al., 1983). The standard CHARMM force field was modified to include both first- and second-order polarization effects induced by the ion on the peptide, using a method described previously (Roux, 1993; Roux et al., 1995). The ion-system interactions are given by

$$E_{i-s} = E_{core} + E_{vdW} + E_{elec} + E_{pol}, \quad (1)$$

where E_{core} is the core repulsion $A^{(8)}/r^8$, E_{vdW} is the van der Waals attraction $-B^{(6)}/r^6$, E_{elec} is a standard electrostatics interaction between the ion and the partial charge of the peptide atoms, and E_{pol} is an ion-induced polarization interaction. In the present approximation, the polarization interaction E_{pol} arises from the interaction between the point dipole induced on the peptide atoms by the ion and all of the other charges in the system. One might refer to this approximation as "excess ion-induced polarization" (i.e., the polarization induced by the other atoms is assumed to be accounted for, at least in an average mean-field sense). In a previous study, the approximation was shown to agree remarkably well with ab initio calculations (Roux, 1993). To first order, the induced dipole μ_i on atom i by the charge q_{ion} of the ion is

$$\mu_i = \alpha_i q_{ion} \frac{(\mathbf{r}_i - \mathbf{r}_{ion})}{|\mathbf{r}_i - \mathbf{r}_{ion}|^3}, \quad (2)$$

where α_i is the atomic polarizability of atom i. The interaction of the induced dipolar with the charge of the ion is

$$E_{pol}^{(1)} = -\frac{1}{2} \sum_i \frac{\mu_i \cdot (\mathbf{r}_i - \mathbf{r}_{ion})}{|\mathbf{r}_i - \mathbf{r}_{ion}|^3} q_{ion}$$

$$= -\frac{1}{2} \sum_i \frac{\alpha_i q_{ion}^2}{|\mathbf{r}_i - \mathbf{r}_{ion}|^4}. \quad (3)$$

To second order, the induced dipoles interact with all other charges q_j in the system:

$$E_{pol}^{(2)} = \sum_{ij} -\frac{\mu_i \cdot (\mathbf{r}_i - \mathbf{r}_j)}{|\mathbf{r}_i - \mathbf{r}_j|^3} q_j. \quad (4)$$

Hereafter, the potential consisting of the sum of first- and second-order polarization, as used in the present study, will be referred to as $E^{(12)}$. The atomic polarizabilities have been given elsewhere (Roux and Karplus, 1991a, 1995). No polarizability was attributed to the water molecules because the interactions of singly charged ions with water can be reasonably well described with standard fixed charge models (Jorgensen and Severance, 1993). Because of the change from PARAM version 19 to version 22, the parameters $A^{(8)}$ and $B^{(6)}$ were readjusted to fit calculated ab initio potential energy surfaces; their values are 6900 and 530, respectively (their previous values were 83,000 and 440; see Roux et al., 1995). The Lennard-Jones parameters σ and ϵ for sodium were fitted to reproduce the correct solvation free energy in bulk water (−100 kcal/mol) (Beglov and Roux, 1994); their values are 0.0469 kcal/mol and 2.429926 Å, respectively. All of the other ion interaction parameters used in the calculation have been have been given elsewhere (Roux et al., 1995).

To construct the initial configuration used in the present investigation, a snapshot of a fully solvated GA:DMPC system (with no sodium) was taken from the study of Woolf and Roux (1996). The initial construction and equilibration of this system have been described in detail elsewhere (Woolf and Roux, 1994; 1996). Briefly, the system was assembled from prehydrated and preequilibrated DMPC molecules selected randomly from a large set of conformers. The number of bad contacts was reduced by performing rigid body rotations and translations of the prehydrated lipid conformers. The initial configuration of the protein-membrane complex was then further refined using energy minimization, and the resulting system was equilibrated with molecular dynamics. A water near 9.3 Å in the channel was substituted by a sodium cation, and the resulting configuration was refined by energy minimization. The system was then equilibrated for 50 ps using molecular dynamics. A molecular graphics representation of the simulation system can be seen in Woolf and Roux (1996).

The nonbonded interaction cutoffs, on all nonsodium interactions, followed the work of Pastor et al. (Venable et al., 1993) on pure lipid bilayers. The electrostatic interactions were smoothly shifted over their entire interaction distance to zero at a cutoff distance of 12 Å. A switching function from 10 to 12 Å was used for the van der Waals interactions. No truncation cutoff was employed for the nonbonded interactions involving the sodium ion to describe the microscopic forces realistically at all distances. Similar mixed cutoffs have been used previously (for example, see Kovacs et al., 1995). The trajectories were calculated in the microcanonical ensemble with constant energy and volume. Although constant pressure algorithms are well established for simulating isotropic liquids, there remains some controversy in applying those methods to membrane systems (Feller and Pastor, 1996; Jähnig, 1996). To avoid those difficulties, the x-y cross section of the GA:DMPC system was carefully estimated (Woolf and Roux, 1996), and a constant-volume method was used. The equa-

tions of motion were integrated using a time step of 2 fs. The length of all bonds involving hydrogen atoms was kept fixed by using the SHAKE algorithm (Ryckaert et al., 1977). The average temperature remained at 340 K, above the gel-liquid crystal phase transition and consistent with experimental conditions (J. Davis, personal communication). All of the calculations were performed using the simulation program CHARMM (Brooks et al., 1983).

Calculation of solid-state NMR properties

Because the time scale of solid-state NMR is much slower than the fast molecular motions, observed properties such as deuterium quadrupolar splittings, dipolar couplings, chemical shifts, and chemical shifts anisotropy result from a time average over rapidly fluctuating quantities. This implies that the nuclear spins evolve according to an effective spin Hamiltonian that can be calculated from a configurational average (Ernst et al., 1987). It is important to emphasize that, because of the nonlinear functional dependence of the NMR observables on the molecular geometry, such an averaging process differs essentially from calculations based on a single average molecular configuration. In particular, the average chemical shifts observed experimentally in directions parallel and perpendicular to the membrane normal (taken to be along the z axis) are, respectively,

$$\langle \sigma_{\parallel} \rangle = \langle \hat{\mathbf{z}} \cdot \sigma(t) \cdot \hat{\mathbf{z}} \rangle, \tag{5}$$

and

$$\langle \sigma_{\perp} \rangle = \frac{1}{2} \langle \hat{\mathbf{x}} \cdot \sigma(t) \cdot \hat{\mathbf{x}} \rangle + \frac{1}{2} \langle \hat{\mathbf{y}} \cdot \sigma(t) \cdot \hat{\mathbf{y}} \rangle. \tag{6}$$

The observed chemical shift anisotropy (CSA) is

$$\langle \Delta\sigma \rangle = \langle \sigma_{\parallel} \rangle - \langle \sigma_{\perp} \rangle. \tag{7}$$

In Eqs. 5 and 6, $\sigma(t)$ is the instantaneous second-rank shielding tensor (Cross and Opella, 1985; Woolf and Roux, 1994; Woolf et al., 1995),

$$\sigma(t) = \sum_{i=1}^{3} \hat{\mathbf{e}}_i(t) \sigma_{ii} \hat{\mathbf{e}}_i(t), \tag{8}$$

where σ_{ii} and $\hat{\mathbf{e}}_i(t)$ are, respectively, the instantaneous magnitude and direction of the principal tensor components, and $\hat{\mathbf{x}}$, $\hat{\mathbf{y}}$, and $\hat{\mathbf{z}}$ are unit vectors.

An important assumption in the present analysis is that the shielding tensor orientation is fixed relative to the local molecular frame and that the component magnitudes are constant (Woolf et al., 1995). The magnitude and orientation of the ^{15}N and ^{13}C chemical shift tensors determined experimentally were used (Nicholson and Cross, 1989; Teng et al., 1992; T. A. Cross, personal communication). The largest component of the ^{15}N chemical shift tensor (196 ppm) lies in the amide plane, almost parallel to the N-H bond, making an angle of 105° with the C-N bond (Teng and Cross, 1989). The largest component of the ^{13}C chemical shift tensor (244 ppm) also lies in the amide plane, in the triangle formed by the O-C-N atoms, making an angle of 38° with C-N bond (Teng et al., 1992). The magnitude and orientation of the backbone carbonyl ^{13}C and ^{15}N shielding tensors are shown in Fig. 1.

The observed ^{15}N-^{1}H dipolar coupling is given by $|\nu_{DC} S^2|$, where ν_{DC} is the standard dipolar coupling constant and S^2 is the average bond order parameter. Assuming a N-H distance of 1.025 Å in the expression $2(h\gamma_N\gamma_H/r_{NH}^3)$, the standard dipolar coupling constant is estimated to be 22.5 kHz (Teng et al., 1991). The average bond order parameter S^2 can be calculated as a time average from a molecular dynamics trajectory:

$$S^2 = \left\langle \frac{3\cos^2(\theta(t)) - 1}{2} \right\rangle, \tag{9}$$

where $\theta(t)$ is the instantaneous angle of the ^{15}N-^{1}H bond with the z axis. By definition, the average bond order parameter can have a maximum of 1.0 ($\theta = 0°$ for all t) and a minimum of -0.5 ($\theta = 90°$ for all t), although only the absolute value $|S^2|$ can be observed experimentally. The quadrupolar splitting of carbon-bound deuterium is given by a similar expression, $|\nu_{DQS} S^2|$, where S^2 is the C-^{2} bond order parameter, and the value of the standard coupling constant ν_{DQS} for a carbon-deuterium bond is 3/2(183) kHz (Hu and Cross, 1995).

Because of the slow NMR time scale, the observed properties correspond to a superposition of dimer channels with zero, one, or two bound sodium ions, with equal contributions from the two identical isotopically labeled monomers. The solid-state NMR experiments were performed with a concentration of 160 mM [NaCl] (Smith et al., 1990). Assuming that the binding constants for singly and doubly

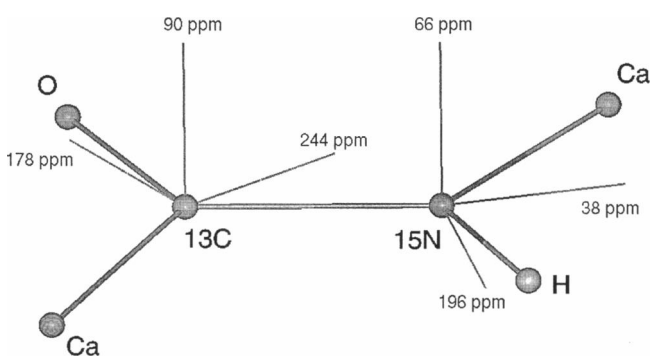

FIGURE 1 Schematic representation of the magnitude and orientation of the ^{13}C and ^{15}N chemical shift tensors of the peptide linkage. The largest component of the chemical shift tensor of the ^{13}C chemical shift tensor (244 ppm) lies in the amide plane, making an angle of 38° with the C-N bond (Teng et al., 1992). The largest component of the chemical shift tensor of the ^{15}N chemical shift tensor (196 ppm) lies in the amide plane, almost parallel to the N-H bond, making an angle of 105° with the C-N bond (Nicholson and Cross, 1989; Teng and Cross, 1989). The magnitudes for the ^{15}N chemical shift of Trp^{11} are shown (T. A. Cross, personal communication).

occupied channels in the oriented GA:DMPC samples are similar to those measured with LPC vesicles (Jing et al., 1995), there should be, on average, one ion present per dimer channel, and the contributions from other occupancy states can be neglected. However, the observed spectra represent the superposition of the ion-bound and the ion-free monomer. It should be noted that the residues of the ion-free monomer are not expected to be strongly affected by the presence of sodium, because the distance between the two binding site is large (they are located approximately at ±9 Å along the channel axis). In particular, at 160 mM [NaCl] the observed deviation of the ^{13}C CSA of Leu^{10} relative to the ion-free channel may be expected to reflect approximately one-half of the total structural perturbation induced in the ion-bound monomer.

The expressions in Eqs. 5–9 represent averages over all possible configurations of the channel in the presence of one sodium. Thus, in principle, the configurational average could be performed by running a single long molecular dynamics trajectory of the solvated GA:DMPC system, including one sodium ion. However, it cannot be expected that a single straight molecular dynamics simulation will be able to efficiently sample all of the relevant configurations during a trajectory of a few hundreds of picoseconds. In particular, the presence of energy barriers may considerably reduce the motions of the ion along the channel axis. To perform the average corresponding to the ion motion along the channel axis, it is necessary to use a computational approach enforcing a biased sampling of infrequent configurations (Roux and Karplus, 1994). Rewriting Eqs. 5 and 6 explicitly in terms of an integration over the channel axis (oriented along z),

$$\langle \Delta\sigma \rangle = \int dz\, \mathcal{P}(z)\, \langle \Delta\sigma(z) \rangle, \qquad (10)$$

where $\mathcal{P}(z)$ is the normalized probability distribution of the ion along the z axis in the singly occupied channel, and $\langle \Delta\sigma(z) \rangle$ is the average CSA in the singly occupied state with the ion fixed at z. A similar spatial z average can be used to express other NMR observables.

The z-dependent averages for all NMR observables were calculated from biased simulations with one sodium constrained at different locations along the z axis in the GA:DMPC system (see below). The backbone carbonyl ^{13}C chemical shift anisotropy, the ^{15}N parallel chemical shifts, and ^{15}N-^{1}H dipolar coupling, as well as the parallel chemical shift of the Trp indole $^{15}N\epsilon 1$ and the deuterium quadrupolar splitting for the Trp side chains, were examined using this approach.

Biased sampling protocol and computational details

To perform the configurational sampling required to evaluate Eq. 10, a set of biased simulations in which the ion was restrained at various positions along the channel axis were generated and analyzed. Harmonic functions of the form $(1/2)k(z - z_i)^2$, centered on successive values z_i, were used to produce the biased trajectories. The configuration for the biased simulations were generated from the initial system with the ion constrained near 9.3 Å. The subsequent windows were generated by translation of the ion along z by 0.4 Å, followed by energy minimization. The windows were equilibrated with 3 ps of Langevin dynamics, using a friction of 5 ps^{-1} on all heavy (nonhydrogen) atoms. The system was then further equilibrated for 3 ps with velocity scaling and by 9 ps of straight molecular dynamics. Data were then collected for the next 25 ps. Initially, a force constant of 2 kcal/mol-Å^2 was used. Three sets of subsequent windows were collected to improve the sampling over the initial set of 11 windows. The second set of seven windows used a force constant of 5 kcal/mol-Å^2 and were generated by displacements from the initial windows of 0.2 Å. The same equilibration procedure was used. A third set of windows used a force constant of 10 kcal/mol-Å^2 and was set up to sample the region from 12.2 to 13.3 Å in five windows. A final fourth window was added at 8.4 Å, with a force constant of 20 kcal/mol-Å^2, to provide the best sampling of ion z-positions from 7.7 to 13.3 Å. In the end, 12,000 configurations taken from the 24 windows were used for the analysis. All of the information generated by the biased simulations was combined to obtain the z-dependent averages by using several programs written specially for the present analysis.

The probability distribution of the singly occupied channel $\mathcal{P}(z)$ is directly related to the free energy profile $\mathcal{W}(z)$ along the channel axis,

$$\mathcal{P}(z) = \mathcal{C} e^{-\mathcal{W}(z)/k_B T}, \qquad (11)$$

where $\mathcal{C}$ is a normalization constant. The umbrella sampling technique (Patey and Valeau, 1975) was used to determine the free energy profile, $\mathcal{W}(z)$, along the z axis. The weighted histogram analysis method (WHAM) was used to unbias the umbrella sampling calculation (Kumar et al., 1992; Roux, 1995). The average properties as a function of z were calculated by using all available configurations from all of the windows. A bin size of 0.25 Å was used in WHAM. To remove translation and rotation along the z axis, the channel configurations were reoriented to best fit a GA reference structure. The purpose of the reorientation was to remove the slow wobble of the channel from the set of final configurations, which was poorly averaged in the present umbrella trajectories.

RESULTS AND DISCUSSION

Solid-state NMR observables

The average properties of the NMR observables as a function of the sodium ion position along the z axis were calculated by combining all of the information generated from the 24 umbrella sampling simulations. The results

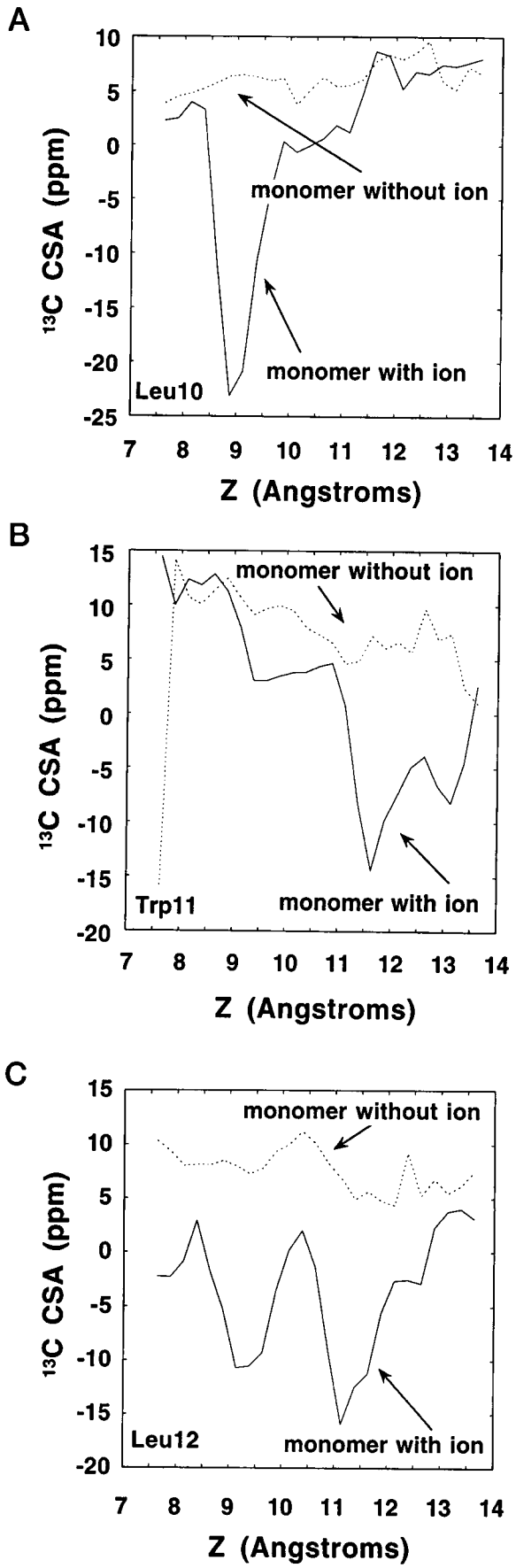

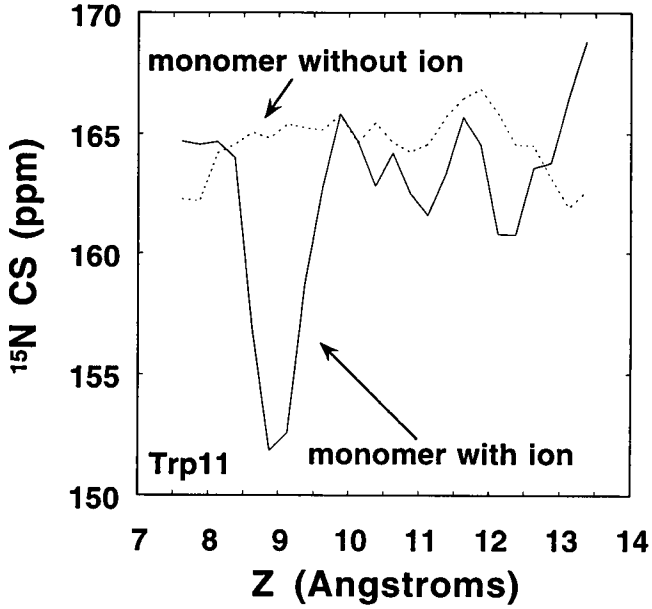

FIGURE 3 ^{15}N chemical shift parallel at the Trp^{11} backbone site as a function of the position of the ion along the z axis. The large CSA shift of Leu^{10} ^{13}C is correlated with a similar shift for the Trp^{11} ^{15}N backbone of the same peptide plane (see Fig. 2).

show variation in the NMR observables as the ion moves along the GA channel axis. These values can be integrated with respect to the z axis, weighted by the probability distribution $\mathcal{P}(z)$ to obtain a single number that can be compared directly to the time-averaged value measured experimentally. Fig. 2 illustrates the ^{13}C CSA as a function of z for three different residues. A large change is seen for the residue Leu^{10} of the monomer containing the sodium ion. This is in contrast to the same residues of the ion-free monomer, which are clearly unaffected. For Leu^{10}, the largest change in the CSA relative to the ion-free channel is observed when the ion is near 9 Å. The CSA is considerably less affected when the ion is at other locations along the channel axis. The calculations indicate that the CSAs of Trp^{11} and Leu^{12} should also be affected when the ion is near 11 Å. In a solid-state NMR experiment, the change in CSA caused by the presence of sodium should reflect the fraction of time spent by a sodium cation at particular positions along the channel axis. For example, if the ion spends a considerable fraction of time near 9 Å, the calculations indicate that the CSAs of Leu^{10} and Leu^{12} would be strongly and moderately affected, respectively, whereas that of Trp^{11} would not be affected.

FIGURE 2 ^{13}C CSA for three backbone sites averaged from the trajectories as a function of the position of the ion along the z axis. The average was obtained from 24 umbrella-sampled windows producing a sampling of cation positions from z of 8–13 Å. The large change occurred at ~9 Å for both Leu^{10} and Leu^{12}. In contrast, the change for Trp^{11} is only occurs z values greater than 11 Å. (The large change at 7.5 Å for the monomer without ion reflects the lack of sampling in that region).

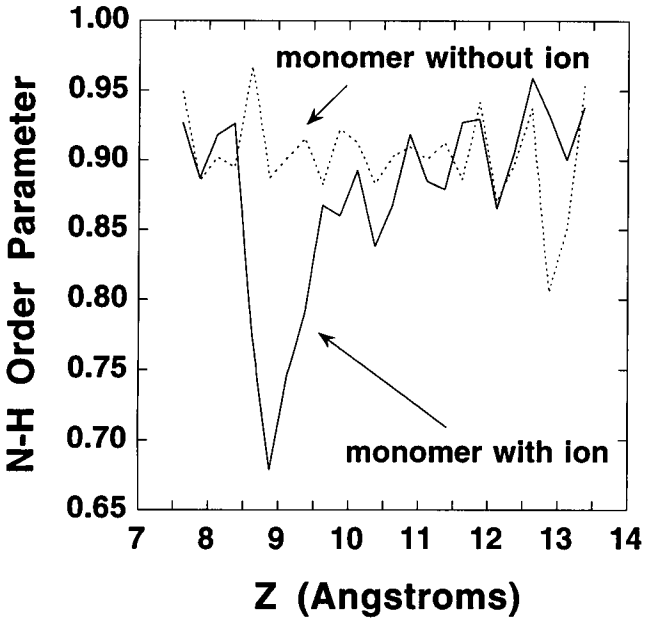

FIGURE 4 Order parameter of the ^{15}N-^{1}H bond averaged over all windows and z positions.

Because of the amide plane structure, correlated changes should be seen at ^{15}N-labeled sites within the same peptide bond. Fig. 3 shows the changes in the ^{15}N backbone site of Trp^{11} as a function of the sodium location along the z axis. There is a large change when the ion is near 9 Å and little change at other locations. This is consistent with the variations in the carbonyl ^{13}C CSA of Leu^{10} shown in Fig. 2. Similarly, the ^{15}N-^{1}H dipolar splitting at all residues due to the cation presence at various z values was computed. Fig. 4 shows the bond order parameter for the Trp^{11} site. The calculations suggest that the maximum change in ^{15}N-^{1}H dipolar coupling occurs when the cation is at 9 Å.

Further calculations were performed to characterize the changes induced by the presence of sodium in the deuterium quadrupolar splittings at backbone Cα, and at the tryptophan residues (chemical shift of indole $^{15}N\epsilon1$, $^{15}N\epsilon1$-$^{1}H\epsilon1$ dipolar coupling, and C-^{2}H deuterium quadrupolar splittings of the indole ring). The calculations predict that there should be no large change as a function of the z position of the cation for each of these other sets of solid-state NMR measurements. This is consistent with experimental data on ^{13}C CSA values for Trp^{9}, Trp^{11}, Trp^{13}, and Trp^{15} at the C$\delta2$ of the indole ring (Smith et al., 1990; Separovic et al., 1994; F. Separovic, personal communication). In particular, the analysis indicates that no large structural changes on the Trp side chains are induced by the presence of an ion in the binding site.

The free energy profile for the ion along the 8–13-Å channel axis reaction coordinate resulting from the 24 umbrella sampling windows is shown in Fig. 5. The profile determines the fraction of time spent by the ion at each z location along the channel axis. For comparison, the free-energy profile calculated previously (PMF-1993) using a

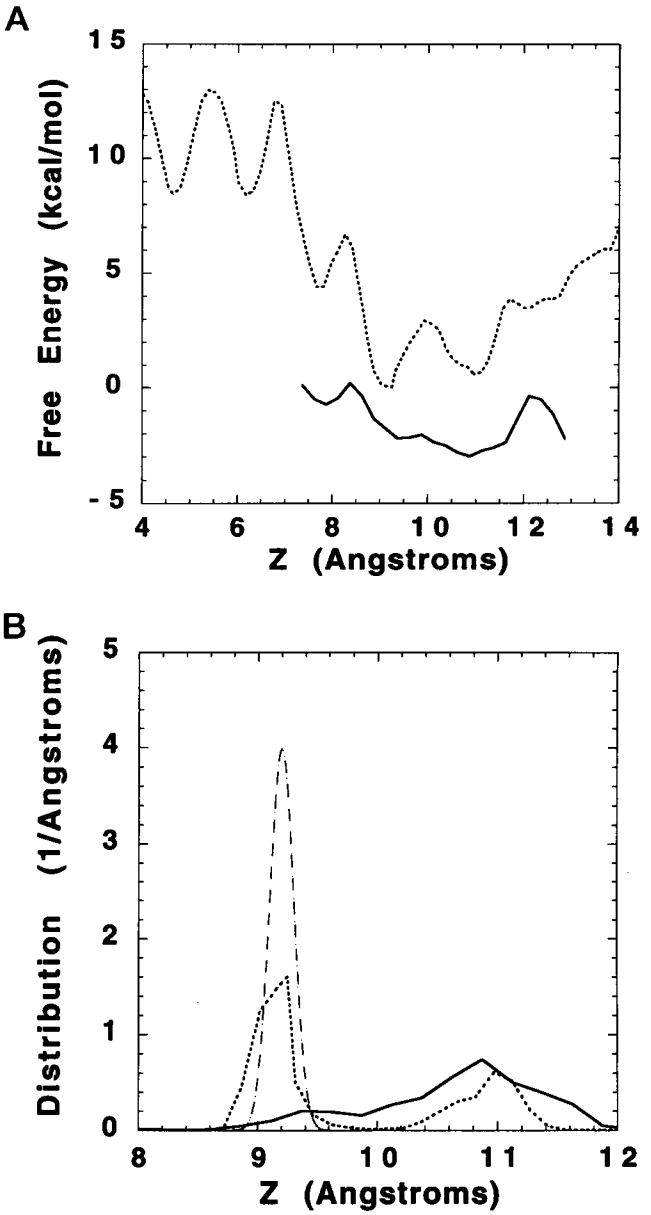

FIGURE 5 (*Top*) Free energy profile (or PMF) $\mathcal{W}(z)$ for the sodium ion along the channel axis determined by the 24 umbrella sampled windows (——). The result suggests three possible binding sites for the sodium ion, with the relative depth of the wells being less well determined than their relative position. ·····, PMF obtained by Roux and Karplus (1993) (the relative vertical energy offset is arbitrary). (*Bottom*) Probability distributions $\mathcal{P}(z)$ corresponding to the free energy profiles. – – –, Gaussian distribution centered at 9.2 Å with a width of 0.1 Å, as used in the empirical analysis. The width of the Gaussian was chosen to match the distribution function arising from a single free energy well in the PMF.

molecular dynamics free energy perturbation technique is also shown (Roux and Karplus, 1993). The wells and barriers of the new and the previous PMF are given in Table 1. Although the general structure of the free-energy profile is similar, it is clear that the two results differ significantly. The present calculation indicates that there are three wells for the ion binding. The first well is roughly around 7.9 Å,

TABLE 1 Comparison of the PMFs

Wells and barriers	New PMF		PMF-1993	
	z	$\mathcal{W}(z)$	z	$\mathcal{W}(z)$
Well 5	7.9	2.3	7.7	4.4
Barrier 5–6	8.4	3.2	8.3	6.7
Well 6	9.4	0.8	9.3	0.0
Barrier 6–7	9.9	0.9	9.9	2.9
Well 7	10.9	0.0	11.0	0.6
Barrier 7*	12.1	2.6	11.8	3.8

*Positions are given in angstroms and energies in kcal/mol; the numbering of the wells follows the description in Roux and Karplus (1993).

the second well is around 9.4 Å, and the third and deepest well is around 10.9 Å. In the PMF-1993 calculation, the deepest free-energy minimum was located near 9.3 Å, with secondary minima at 7.7 and 11.0 Å. Although the Lennard-Jones parameters of the ion were adjusted empirically to reproduce the solvation energy of sodium in bulk water, it seems that the ion is too strongly attracted to the bulk water at 12 Å and beyond. This might be due to the neglect of induced polarization on the water molecules. Interestingly, the free energy barriers separating the three wells are much smaller in the present calculations. Recent analysis of ion flux data based on the Nernst-Planck diffusion equation suggests that the activation barrier of PMF-1993 is too large (McGill and Schumaker, 1996). Therefore, the reduced activation free-energy barrier found in the present calculations, which corresponds to faster ion translocation, appears to be in better qualitative accord with experimental ion flux data.

The change in relative stability between the wells at 9.2 and 10.9 Å results from an interplay of a large number of complex factors. In the previous PMF-1993 calculation, the channel was solvated by using 190 water molecules, and a model membrane made of nonpolar spheres was included. In the present calculation, the microscopic environment is more realistic because a fully solvated phospholipid bilayer membrane was explicitly included. The PMF-1993 was calculated using PARAM19 (Brooks, 1983), an extended atom force field (nonpolar hydrogens are represented as part of the heavy atom to which they are attached), augmented to account for first-order ion-induced excess polarization. In the present calculations, the all-atom PARAM22 of CHARMM was used, and both first- and second-order polarizations were taken into account. First-order polarization, such as that included in the calculation of PMF-1993, results in a pairwise additive attractive interaction, whereas second-order polarization represents a non-pairwise-additive contribution to the potential energy function (Roux, 1993). It has been shown by comparison with ab initio calculations that the second-order approximation retains the dominant nonadditive contributions (Roux, 1993). Second-order effects give rise to an effective reduction of the ion affinity for the backbone carbonyl groups of the channel (Roux, 1993). Nonadditive second-order polarization energy was found to be necessary to obtain the correct magnitude for the absolute free energy of Na^+ in the channel; its contribution amounts to almost 40% of the total free energy (Roux et al., 1995). The extended atom PARAM19 and the all-atom PARAM22 force fields differ for the nonbonded (Lennard-Jones radii and partial charges) as well as for the internal energy terms (bond, angle, and dihedral force constants). It is beyond the scope of the present paper to make a complete quantitative assessment of all these factors. However, despite the considerable differences between the microscopic model and the potential function, the two PMFs are qualitatively similar.

To perform the time average corresponding to the NMR observations, it is necessary to perform a Boltzmann-weighted average using the PMF of the ion at various positions along the z axis. The probability distributions corresponding the two PMFs are shown in Fig. 5. As shown in Table 2, the calculated CSAs, based on the spatial averaging provided directly from the PMF calculated by molec-

TABLE 2 ^{13}C CSA values*

Residue	Calculated ^{13}C CSA			Observed ^{13}C CSA		
	Ion-free	With sodium	−change	Ion-free	With sodium	−change
Val^{1}	6.4	4.1 (3.7)	2.3 (2.7)			
Gly^{2}	8.5	7.7 (9.0)	0.8 (−0.5)	11.0	11.0	0.0
Ala^{3}	6.8	6.9 (5.7)	−0.1 (1.1)	14.0	14.0	0.0
Leu^{4}	11.5	11.7 (11.9)	−0.2 (−0.4)	12.0	12.0	0.0
Ala^{5}	6.3	5.0 (5.5)	1.3 (0.8)			
Val^{6}	11.1	11.6 (11.5)	−0.5 (−0.4)			
Val^{7}	8.4	8.7 (10.3)	−0.3 (−1.9)	16.0	16.0	0.0
Val^{8}	13.0	12.4 (11.6)	0.6 (1.4)			
Trp^{9}	14.6	14.9 (15.1)	−0.3 (−0.5)			
Leu^{10}	8.5	4.6 (−2.9)	3.9 (11.4)	9.0	0.0	9.0
Trp^{11}	2.3	−1.4 (2.0)	3.7 (0.3)	10.0	10.0	0.0
Leu^{12}	6.4	0.2 (0.0)	6.2 (6.4)	12.0	7.0	5.0
Trp^{13}	7.8	6.5 (7.9)	1.3 (−0.1)	10.0	10.0	0.0
Leu^{14}	9.6	7.4 (8.3)	2.2 (1.3)	13.0	7.0	6.0
Trp^{15}	−7.9	−3.5 (3.9)	−4.4 (−4.0)			0.0

*The numbers in parentheses were calculated using a Gaussian of width 0.1 Å centered at 9.2 Å to represent the distribution function $\mathcal{P}(z)$.

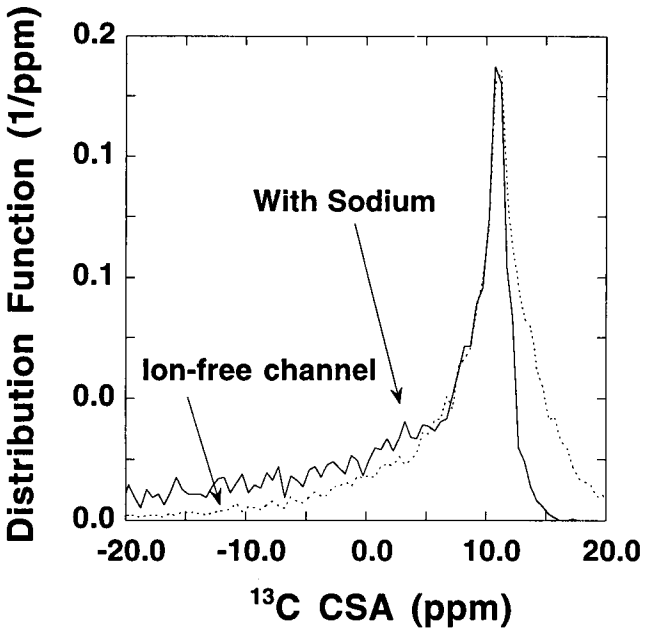

FIGURE 6 Distribution of possible ^{13}C CSA values for the water-filled and the singly occupied channel. The observed experimental CSA is a time average over the distribution of possible values. With the cation present, the CSA shifts to a broader tail. When both sides are averaged together, the original sharp peak at 10 ppm is reduced and broadened.

ular dynamics, are not in excellent agreement with the observed values. The reason is that very small deviations in the calculated PMF lead to very large variations in the probability distribution of the sodium ion in the channel entrance which, in turn, influences the outcome of the weighted average NMR properties. The free-energy well at 11.0 Å is only slightly deeper than the one near 9.3 Å; as shown in Table 1, the relative free energy of the two wells near 9.3 and 11.0 has only changed from +0.6 (PMF-1993) to −0.8 kcal/mol (new PMF). However, this is sufficient to influence considerably the average process. The present situation highlights the limitations of current computational models and force fields. Because of their sensitivity to the details of the microscopic computational model, properties involving energetic factors such as a free energy profile are difficult to obtain accurately. Nevertheless, to interpret the available solid-state NMR data in terms of the location of the sodium binding site, it is the z dependence of the solid-state NMR properties rather than an absolute prediction of the energetics of binding that is of interest.

A semiempirical approach combining all available information from both the simulations and the experiments was used to find the most plausible location of the major sodium-binding site. The empirical procedure we propose is very similar in spirit to that used to deduce a proton-proton distance by interpreting the interproton nuclear Overhauser effect (NOE) cross-relaxation rate observed by high-resolution NMR (Brooks et al., 1988). A similar semiempirical approach has also been employed to analyze the magnitude of the internal motion of proteins by empirically adjusting the amplitude of calculated normal mode displacement vectors to reproduce the experimental N-H NMR backbone order parameters (Brüschweiler, 1992). In the present case, the position of the ion binding site was deduced by empirically matching the magnitude of the observed CSA. For simplicity, the probability distribution of the sodium along the channel axis was assumed to be a single Gaussian of width 0.1 Å centered at z_0 (the width was chosen to match the distribution function arising from a single free-energy well in the PMF). The position of the Gaussian was then empirically optimized to yield the smallest mean squared deviation between the calculated and observed carbonyl ^{13}C CSA observed by solid-state NMR:

$$\chi^2 = \sum_{\text{labeled residues i}} [\langle \Delta\sigma^i \rangle_{\text{obs}} - \langle \Delta\sigma^i(z_0) \rangle_{\text{calc}}]^2. \quad (12)$$

The best match was found when the Gaussian was centered at 9.2 Å. The resulting Gaussian distribution is shown in Fig. 5. All of the experimental carbonyl ^{13}C CSAs were used for the fit. Table 2 presents the average sodium shifts for ^{13}C at all residues calculated with the best Gaussian. The results of Table 2 show that the change in CSAs are consistent with a sodium-binding site near 9.2 Å. In the following, the structural properties of the major sodium-binding site are analyzed.

Before analyzing the structure of the binding site, it should be emphasized that even small structural fluctuations such as peptide librations may have a significant influence on the interpretation of the solid-state NMR properties in terms of a single average structure. To illustrate this point, a simulation of 100 ps was performed with the ion restrained near the main binding site. On Fig. 6 the relative distribution of the instantaneous values of the ^{13}C CSA for Leu^{10} in the presence of a sodium ion are compared with the same property extracted from a previous simulation of an ion-free channel (Woolf and Roux, 1996). It is observed that the change in the overall distribution is relatively subtle. In both cases, the most frequent value for the CSA corresponds to a sharp peak. The distribution is slightly broader in the presence of an ion. This comparison illustrates how the NMR observables result from a dynamical average over multiple conformations. The presence of an ion alters the distribution of the spontaneous fluctuations of the channel, suggesting that the observed change in CSA relative to the ion-free channel is partly caused by a change in the peptide fluctuations. This example highlights the importance of a change in dynamic motional amplitude and its influence on the interpretation of the solid-state NMR data in terms of a single average structure.

Structure of the sodium-binding site

To obtain more information on the structure of the main site, the molecular dynamics trajectory of 100 ps was generated with the ion restrained at 9.2 Å with a harmonic potential. Average structural properties are given in Table 3. A representative configuration extracted from the simulation is

TABLE 3 Ligand structure of the sodium-binding site

	Ion-oxygen distance (Å)				
	PARAM22*			PARAM19#	
Ligands	$E^{(12)}$	$E^{(1)}$	LJ	$E^{(12)}$	$E^{(1)}$
Val^{8}	3.01	2.41	3.21	2.54	2.28
Leu^{10}	2.84	2.40	2.44	2.41	2.28
Trp^{13}	3.77	2.73	3.02	3.49	2.32
Trp^{15}	2.39	2.29	2.31	2.41	2.27
Water (single-file)	2.31	2.32	2.29	2.26	2.24
Water (bulk)	2.36	2.43	2.28	2.27	2.27

*Averages with $E^{(12)}$ were obtained from a 100-ps trajectory of the GA:DMPC system using PARAM22 with the ion restrained near the binding site; averages with $E^{(1)}$ and LJ were obtained from a 5-ps dynamics.
#Averages with $E^{(12)}$ and $E^{(1)}$ were obtained in a previous study using PARAM19 with a model membrane (Roux, 1993).

shown in Fig. 7. In the binding site the sodium is lying off-axis, making contacts with the carbonyl oxygen of Val^{8}, Leu^{10}, Trp^{15}, and two single-file water molecules. There are no large distortions of the channel structure due to the presence of the ion. The carbonyl group of the Leu^{10}-Trp^{11} amide plane exhibits the largest deviation from the ion-free channel structure. The angle between the C=O bond and the bilayer normal as a function of the sodium position is shown in Fig. 8. For Leu^{10} the changes are most pronounced around 9 Å. The largest deflection of the C=O is around 15°. The carbonyl of Leu^{12} is deflected by 8–10° when the ion is at 9 Å or 11 Å. The entire Leu^{10}-Trp^{11} peptide plane is influenced by the presence of the cation. On Fig. 9 the angle between the N-H bond and the normal to the bilayer is shown as a function of sodium position. For Trp^{11}, the largest change occurs near 9 Å and is on the order of 10–12°. The backbone dihedral angles surrounding the Leu^{10}-Trp^{11} peptide plane are those most affected by the presence of the ion. The $\psi 10$ and $\phi 11$ dihedral angles deviate, respectively, from the standard values for a β-helix, which are -108 and $-111°$ (Roux and Karplus, 1991a), to -126 and $-94°$. The root mean squared (rms) dihedral fluctuations are on the order of 10° with and without ion. The O-C-N-H transpeptide dihedral angle ω deviates from planarity in the presence of an ion. It varies from $-179°$ to $-174°$, with rms fluctuations on the order of 8°C. The deviation from planarity is consistent with the observed difference of nearly 5–10° in the angle distribution of the C=O and N-H bonds relative to the channel axis shown in Figs. 8 and 9. Nevertheless, the channel distortion upon sodium binding is very localized. In particular, the β-helical hydrogen bonding pattern is not strongly perturbed by the presence of the sodium in the binding site. As described previously (see Roux and Karplus, 1993), the main backbone C=O $\cdots$ H-N hydrogen bonds are C=O_i to H-N_{i+7} for even i and C=O_i to H-N_{i-5} for odd i. Thus Val^{8}-Trp^{15}, Trp^{13}-Val^{8}, and Trp^{15}-Leu^{10} form the backbone C=O $\cdots$ H-N hydrogen bonds near the sodium binding site. In the β-helical structure, the C=O group of Leu^{10} is the first carbonyl group pointing toward the bulk with no amide H-N partner to form a hydrogen bond along the β-helix (i.e., there is no residue number 17 with a N-H amide group to provide a hydrogen bonding partner). For this reason, the carbonyl group of Leu^{10} at the channel entrance is able to provide a ligand for a cation without losing a backbone hydrogen bond, which is energetically unfavorable. The loss of a backbone hydrogen bond is partly responsible for the activation free-energy barriers in the interior of the channel (Roux and Karplus, 1991a). In addition, the carbonyl of Leu^{10} is more shielded by the channel structure than those of Leu^{12} and Leu^{14} (which also point toward the bulk and have no N-H hydrogen bonding partner) and thus is considerably less exposed to the surrounding bulk solvent. One might speculate that the particular properties of the carbonyl group of Leu^{10}, a C=O shielded from the surrounding bulk providing a favorable cation ligand without breaking a β-helical hydrogen bond, might be the reason for the existence of a favorable binding site near the GA channel entrance. Other complex factors may also play a role. For example, the nearest water molecule in contact with the ion on the bulk side forms a good hydrogen bond with the carbonyl of Leu^{10} (see Fig. 7).

To illustrate the importance of the ion-induced polarization interactions, a computational experiment was done. An initial configuration of the channel with a sodium at the binding site near 9 Å was extracted from the present simulations. An energy minization was performed, and a short trajectory of 5 ps was generated during which only the first-order polarization $E^{(1)}$ was included (the second-order polarization in Eq. 4 was omitted). A second system was generated in a similar way, using the nonbonded energy terms typically found in biomolecular force fields (i.e., Coulomb and 6–12 Lennard-Jones interactions). The resulting average ion-ligand distances are given in Table 3. Although the ion and the channel retained their overall configuration, the ligand structure around the sodium is sensitive to the detail of the potential function. The largest distortion of the backbone conformation is observed when only first-order polarization is included. The backbone dihedral angles $\psi 10$ and $\phi 11$ changed, respectively, from -126 and $-94°$ to -146 and $-79°$, and the peptide plane dihedral angle ω changed from -174 to $-171°$, deviating even further from planarity than in the previous simulations, which included both first- and second-order polarization.

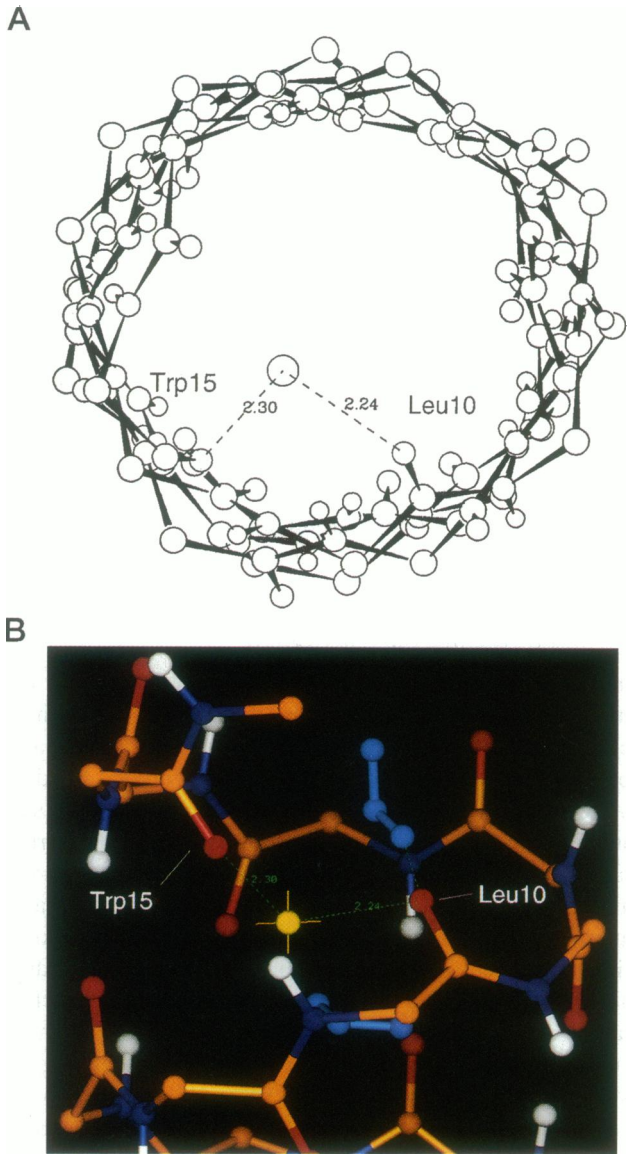

FIGURE 7 Side (*color*) and top (*black and white*) views of the sodium ion at the binding site near 9.2 Å. For clarity, only the backbone atoms and the two nearest single-file waters are represented.

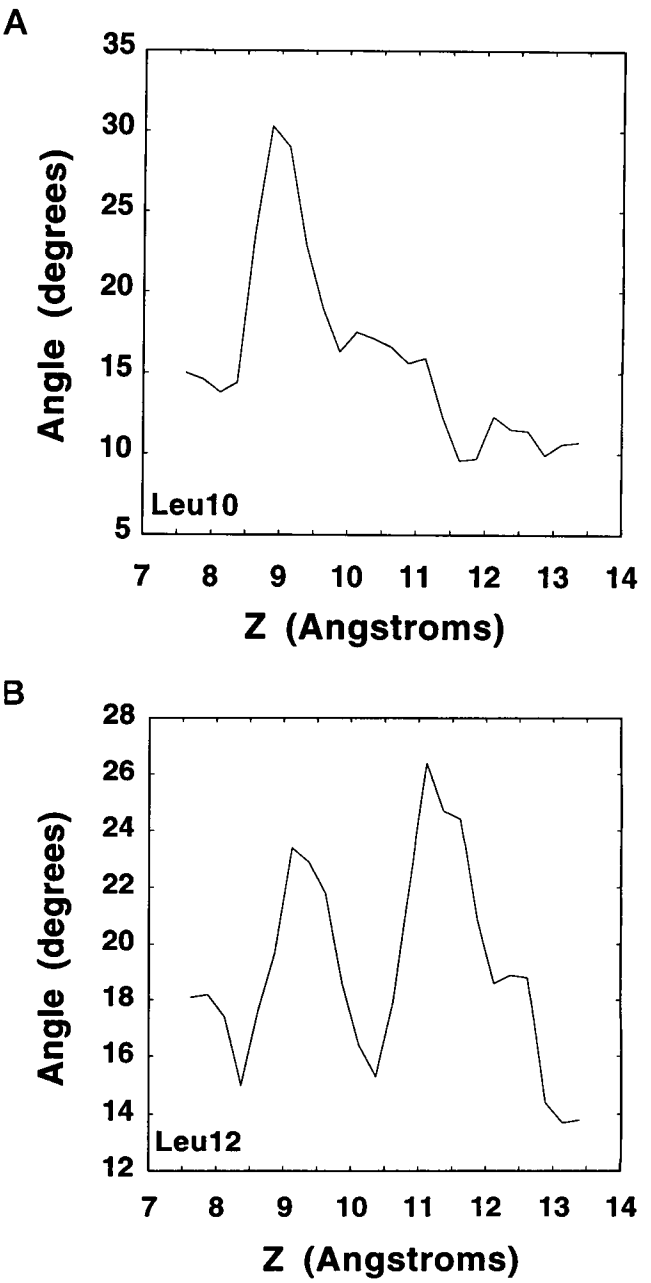

FIGURE 8 The change in ^{13}C CSA values is correlated with variations in the backbone C═O angle with respect to the bilayer normal. This figure shows that when the ion is near 9.2 Å, the angle for the Leu^{10} site has changed by 15° from its unperturbed state. The Leu^{12} site has smaller variations at 9 Å, and at 11 Å.

The rms fluctuations of the dihedrals decreased by 7–9°, indicating that the ligand structure around the ion is more rigid. Furthermore, all of the ion-oxygen distances are shorter when second-order polarization is omitted. In fact, even the number of backbone carbonyls surrounding the ion is changed when second-order polarization is neglected. The distances with the single-file waters are also slightly affected. The observation of stronger interactions with a larger carbonyl ligand is consistent with the overestimated activation barriers found in the PMF-1993, which included only first-order ion-induced polarization.

For comparison, the results obtained with first- and second-order polarization using PARAM19 in a previous study (Roux, 1993) are also shown in Table 3. It is observed that the ligand structure has both similarities and differences. The sodium was stable in the binding site at 9.2 Å in all of the PARAM19 calculations. A harmonic restraint was needed in the current PARAM22 calculations to prevent a drift of the ion toward a more stable position at 11.0 Å. The difference in ion-water distances reflects the change in the

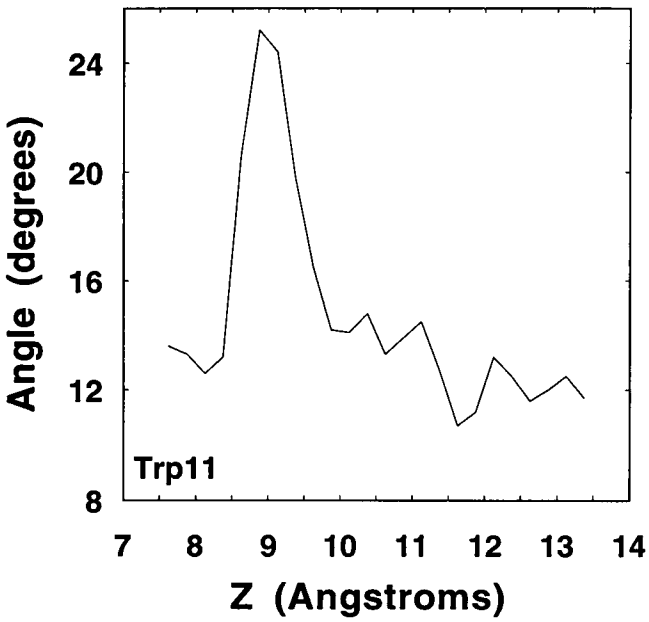

FIGURE 9 The conformational change induced by the ion reflects movement of the whole peptide plane, as is emphasized in this figure showing the change in the N-H angle with respect to the bilayer normal. For the Trp^{11} N-H bond, the angle changes by about 11° when the ion is near the 9 Å binding site.

Lennard-Jones parameters of the ion-water potential (they have been modified to better match the solvation free energy of sodium in bulk water). It appears that even with second-order polarization, the distance between the ion and the carbonyl oxygens is smaller for PARAM19 than PARAM22. The ion-ligand distances are systematically shorter in the case of PARAM19 with only first-order polarization. This suggest that the overestimated free energy barriers in PMF-1993 were probably caused by the neglect of nonadditive polarization. A limited but important conclusion is that the detailed ligand structure of the binding site is very sensitive to the microscopic potential function. In particular, the ion-carbonyl distance and, correspondingly, the tilt of the carbonyl groups stabilizing the ion depend markedly on the nonadditive effects. Interestingly, the results obtained with the standard biomolecular force field are somewhat intermediate. The number of ligands is similar to that of second-order polarization, although the distances are slightly shorter. The backbone dihedral angles $\psi 10$ and $\phi 11$ are, respectively, -142 and $-79°$, and ω is $-172°$. However, it should be stressed that a simple nonpolarizable potential function with Lennard-Jones and fixed partial charge underestimates the interaction of a sodium ion with *N*-methylacetamide by about 5 kcal/mol, based on ab initio calculations (Roux and Karplus, 1995).

Influence of the tryptophan side chains

The determination of the sodium-binding site near the channel entrance using the combined information from solid-state NMR and molecular dynamics simulations provides more information in the attempt to understand the influence of the tryptophan side chains on the channel conductance. It has been observed experimentally that single substitution of any of the tryptophans (9, 11, 13, and 15) by phenylalanine has an important effect on the conductance of the GA channel (Becker et al., 1991). One hypothesis is that the dipole of the indole rings contributes to the the energy profile of an ion moving along the channel axis. However, the data indicate that the four tryptophans do not have the same influence on the measured conductance; substitution of Trp^9 or Trp^{11} reduces the channel conductance from 15 pS to ~2–3 pS, whereas substitution of Trp^{13} or Trp^{15} reduces the channel conductance to ~10–12 pS. A single Trp-to-Phe substitution should result in a small perturbation of the channel structure and of the native free energy profile of a permeating cation. The dipole of the indole ring is mostly due to the Nε1-Hε1 group. Because all four tryptophans are located near the membrane surface, the observed differences in the conductance of chemically modified channels raise important questions concerning the origin of the effects. Despite its imperfections, the present model can serve to bring together several independent piece of information concerning the position of the binding site, the ion flux data, and the influence of Trp on the conductance.

In a rigorous treatment, the contribution of each of the four tryptophans to the free energy profile of sodium in the channel should be calculated using the mean force decomposition technique described previously (Roux and Karplus,

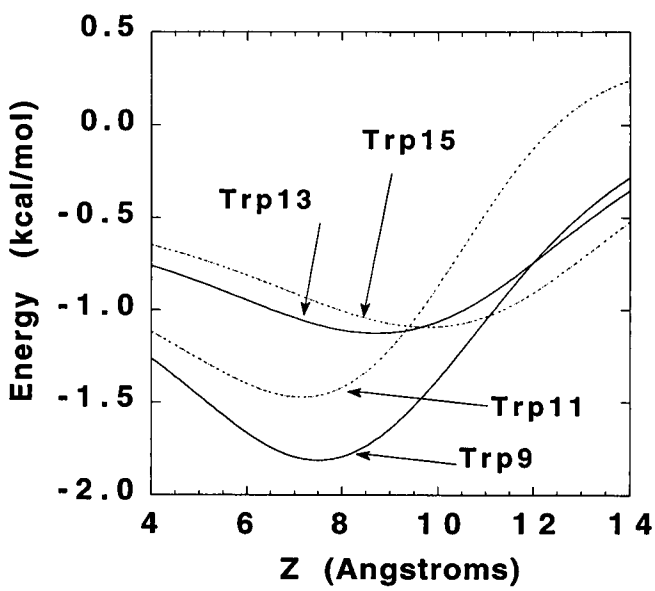

FIGURE 10 The average contribution of the Trp residues to the electrostatic potential along the channel axis (average obtained from a previous simulation (Woolf and Roux, 1996) of the water-filled channel in the absence of sodium ion). The free energy profile obtained from the present simulations (——) and the PMF obtained by Roux and Karplus (1993) (– – –) are shown. The calculations suggest that the dominant effect of Trp^9 and Trp^{11} could be on the first internal free energy barrier (starting near 9 Å), whereas that of Trp^{13} and Trp^{15} could be near the channel mouth.

1991a, 1993); a decomposition of the friction acting on the ion could also be carried out in a similar fashion (Roux and Karplus, 1991b). However, a complete analysis of the Trp-to-Phe substitutions using a fully solvated explicit phospholipid bilayer model would be computationally prohibitive and is beyond the scope of the present study. Nevertheless, because the present analysis indicates that the orientation and conformation of the tryptophan side chains are not strongly influenced by the presence of a cation in the binding site, it is possible to gain some insight using the results of a ion-free simulation of the GA:DMPC system (Woolf and Roux, 1994, 1996). Analysis of the ion-free trajectory showed that the tryptophan side chains were fluctuating around unique conformations, with the N-H group indole pointing toward the bulk solution. The calculated ^{15}N chemical shift, N-H dipolar coupling, and the deuterium quadrupolar splittings of the tryptophan indole ring were in excellent agreement with available solid-state NMR data, indicating that the orientation of the side chains at the membrane-solution interface is essentially correct (Woolf and Roux, 1994, 1996).

The contribution of the tryptophan side chain to the average electrostatic potential energy along the channel axis calculated from a 500-ps trajectory without ions reported previously (Woolf and Roux, 1994, 1996) is shown in Fig. 10. The electrostatic energy profile was averaged over all of the conformations and symmetrized about $z = 0$ to reflect the symmetry of the GA channel. The results are suggestive. In all cases, the magnitude of the electrostatic potential due to the indole dipoles is relatively small (around -0.5 kcal/mol near the minimum). The dominant electrostatic contribution from Trp^9 and Trp^{11} is near 6–8 Å, where the first free energy barrier for sodium permeation is localized along the channel axis. In contrast, the dominant electrostatic contributions from Trp^{13} and Trp^{15} are localized near the channel entrance. Thus it seems plausible that their substitution by Phe would have a smaller impact than Trp^9 and Trp^{11} on the translocation rate of an ion inside the channel.

The present analysis, based on the average electrostatic potential energy arising from the indole ring, is rather crude and neglects the influence of the surrounding environment on the cation free-energy profile. The average electrostatic energy reflects only one component of the exact free energy profile. An exact treatment would require the calculation of the total mean force acting on a cation. In particular, the present analysis could be affected by the ability of the tryptophan side chain to form hydrogen bonds with water or phospholipid molecules through the Nϵ1-Hϵ1 group of the indole ring. It has been observed in a previous study that Trp^{13} and Trp^{15} have a high probability of forming such hydrogen bonds, whereas Trp^9 and Trp^{11} have a low probability (Woolf and Roux, 1996). Therefore it is likely that the average electrostatic potential of the indole ring provides a good estimate of the perturbation of the free-energy profile in the case of Trp^9 and Tr^{11}, whereas the exact influence of Trp^{13} and Trp^{15} may be even smaller than reflected in the present calculations.

Clearly, the influence of side-chain substitution on the conductance of the GA channel depends on both the magnitude of the perturbation and its relation to the unperturbed free energy profile of the native channel. In particular, the perturbed channel conductance is different, whether the main contribution of an indole dipole affects the native free energy profile at the bottom of a well or at the top of an activation barrier (Woolf and Roux, 1997). Although the average electrostatic contribution from the tryptophan side chain depends on both the location and the orientation of the four indole dipoles (on average, the indole Nϵ1 Trp^9, Trp^{11}, Trp^{13}, and Trp^{15} are located, respectively, around 9, 10, 11.5, and 12.5 Å along the channel axis), their substitution by phenylalanine affects the free-energy profile in regions of very different character (wells or barriers). Such considerations should be taken into account in future analyses of the ion flux data to interpret the side-chain substitution experiments. Last, the discussion serves to illustrate the significance of perturbations of the conductance introduced by site-directed mutagenesis and the difficulty to draw conclusions about the structure of biological channels based on such information.

CONCLUDING DISCUSSION

In this paper we have presented an analysis of the sodium-binding site using molecular dynamics simulations for an atomic model of the GA channel embedded in a fully solvated explicit DMPC bilayer. Twenty-four molecular dynamics windows collected with a sodium ion restrained to different axial positions near the presumed sodium-binding site of the GA channel were analyzed to calculate the backbone solid-state NMR properties. Efforts were made to describe the interactions realistically. The nonbonded interactions involving the ion with the rest of the system were not truncated, and the first- and second-order ion-induced polarizations were included. Despite these efforts, the calculated free-energy profile does not appear to be in agreement with experiment. In a previous calculation based on the CHARMM force field PARAM19, the free energy profile showed a minimum at 9.3 Å (Roux and Karplus, 1993), whereas the results of the present calculations have the lowest free energy minimum near 10.5 Å. Although the variation is due to a difference of ~1 kcal/mol, this is sufficient to significantly modify the equilibrium average. Such small variations in the free-energy profile can have an important consequence for the structural average based on the free-energy profile and on the calculation of the translocation rate (Roux and Karplus, 1991b). Because the water and peptide potential functions were developed as effectively pairwise additive functions with nonadditive many-body effects incorporated in an average sense, only the ion-induced polarization was included explicitly (MacKerell et al., 1992; Schlenkrich et al., 1996). However, because of a combination of complex factors, the main binding site has shifted toward the bulk water in the present

calculations. It is possible that limiting the induced polarization to the peptide may have caused an imbalance in the ion-peptide and ion-water interactions. A true self-consistent treatment of polarization applied to the entire system might be able to provide a better representation of the microscopic interactions. These problems illustrate the difficulties in attempting to obtain quantitative accuracy in detailed atomic molecular dynamics simulations of an ion in a transmembrane channel.

Because the resulting averages depend exponentially on the calculated free-energy profile, i.e., $\mathcal{P}(z) \propto \exp[-\mathcal{W}(z)/k_B T]$, a quantitative agreement between the calculation and the experimental structural data is very difficult to achieve. Small variations in the free-energy profile result in a large change in the NMR observables. Therefore, in the present case it is the analysis of the z dependence of the solid-state NMR properties rather than an absolute prediction that is of interest. A semiempirical approach was used in which the probability distribution of the sodium along the channel axis was approximated by a single Gaussian. Its location was optimized to match all available data. The main conclusion is that the analysis of the ^{13}C CSA data using the molecular dynamics calculations provides strong support for the contention that the main binding site for sodium cations in the GA channel is near 9.2 Å (see Table 1). The CSA is largest for ^{13}C-labeled Leu^{10} than for any other residue. This location is in agreement with results from low-angle x-ray scattering (Olah et al., 1991). It was found to correspond to the lowest free-energy minimum in a previous determination of the PMF along the channel axis (Roux and Karplus, 1993). The position is also remarkably consistent with estimates based on current-voltage measurements (Andersen and Procopio, 1980; Eisenman and and Sandblom, 1983; Busath and Szabo, 1988; Becker et al., 1992). The influence of the tryptophan side chains on the channel conductance was examined using the current information about the binding site. According to our analysis, the dominant average electrostatic contributions from Trp^9 and Trp^{11} are localized near the first free-energy barrier, whereas those from Trp^{13} and Trp^{15} are localized near the binding site at the channel entrance. Thus it may be expected that substitutions of Trp^9 and Trp^{11} by Phe might have a bigger effect on the channel conductance as observed experimentally (Becker et al., 1991).

One important approximation in the present analysis is that the shielding tensor orientation is fixed relative to the local molecular frame and that the component magnitudes are constant (see Woolf et al., 1995). Thus our interpretation of the chemical shifts is based entirely on changes in the nuclear degrees of freedom. Of course, the presence of a cation may also induce chemical shifts by perturbing the electronic structure around the ^{13}C and ^{15}N nuclei. Recent ab initio density functional calculations for the electronic changes to be expected in the presence of a sodium ion in the 9.2 Å binding site suggest variations due to electronic structure that could act in combination with the nuclear conformational changes observed in the current molecular dynamics calculations (Woolf et al., unpublished calculations). In addition, recent experiments reveal that electronic effects on the observed chemical shifts due to the presence of the ion are important (T. A. Cross, personal communication). Those recent results show that the chemical shift of ^{15}N-labeled Trp^{11} is changed by 3–4 ppm because of the presence of sodium. This is in qualitative accord with the present calculations of the ^{15}N-labeled Trp^{11}, which yields a change of 4–5 ppm using the best-matching Gaussian centered at 9.2 Å. It is also observed that the backbone ^{15}N-^2H dipolar coupling values change by only 6% at high sodium concentrations corresponding to double ion occupancy, indicating that the channel structure is only slightly affected by the presence of sodium in the binding site (T. A. Cross, personal communication). The maximum estimated distortion corresponds to approximately 5°. In contrast, the current calculations suggest a deflection of the N-H bond in the range of 9–10° using the best-matching Gaussian centered at 9.2 Å. The discrepancy might be due to a combination of subtle factors other than the neglect of electronic effects on the chemical shielding tensor, or inaccuracies in the potential function. For example, it is conceivable that, whereas a first ion binds at ± 9.2 Å, a second binds at ∓ 10.9 Å, giving rise to a nonsymmetrical situation (Jing et al., 1995), which would make the interpretation of the NMR data more difficult. In fact, at 160 mM [NaCl] the influence of double occupancy is possible; from the binding constant 167 M^{-1} and 1.7 M^{-1} (Jing et al., 1995), there could be 85% and 12% singly and doubly occupied channels, respectively. Moreover, small deviations from planarity of the peptide linkage Leu^{10}-Trp^{11} may lead to inconsistencies in the interpretation of the solid-state NMR data in terms the orientation of the C=O and the N-H groups. To otain more information on the orientation of the peptide linkage, a possible though difficult experiment would be to observe the ^{13}C-^{19}O dipolar coupling at the Leu^{10} site using solid-state NMR. Last, the orientational fluctuations of the backbone N-H bond may have been affected because the dynamic equation of motions was integrated with fixed length for all of the bonds involving hydrogen atoms using the SHAKE algorithm (Ryckaert et al., 1977). Nevertheless, the qualitative agreement between the calculations and the experiments is satisfactory.

In previous calculations it was observed that the sodium ion was establishing strong contacts with four carbonyl oxygens (Leu^{10}, Trp^{15}, Val^8, and Trp^{13}) and with two single-file water molecules (Roux and Karplus, 1993). Although a similar ligand structure is observed in the present calculations, it is significantly more flexible because of the incorporation of second-order polarization (see Table 3). In the binding site, the sodium ion is lying off-axis, and the main ligand is provided by the carbonyl group of the Leu^{10}-Trp^{11} peptide plane (see Fig. 7). Transient contacts with the carbonyl group of Val^8 and Trp^{15} are also present. Because it is undergoing the largest structural deviation, the Leu^{10}-Trp^{11} peptide plane exhibits the largest CSA upon cation binding. Furthermore, the calculations indicate that the pep-

tide linkage can deviate slightly from planarity in the presence of the cation. These observations suggest that the movements of sodium ion through the GA channel do not involve simple interactions with a fixed and static structure. Last, it should be emphasized that the configurations with the ion in the binding site near 9.2 Å strongly dominate the time average corresponding to the observed NMR properties. However, larger structural distortions could occur during the permeation process as the ion is crossing free-energy barriers (e.g., between 8.5 and 9.0 Å along the channel axis). Because of their smaller statistical weight, configurations with the ion at the top of a free energy barrier do not contribute significantly to the time average, giving rise to the solid-state NMR properties. They may thus remain undetected experimentally. It is our hope that a better understanding of the permeation process will be achieved by using a combination of experimental data and molecular dynamics simulations.

We thank T. A. Cross for sharing data before publication and for many useful discussions. These results are now published (Tian et al., 1996). We are grateful to David Busath for useful suggestions.

This work was initiated while TBW was a postdoctoral fellow in the Membrane Transport Research Group. Their financial support is gratefully acknowledged. BR is a Research Fellow of the Fonds de Recherche pour la Santé du Québec (FRSQ).

REFERENCES

Andersen, O. S., and R. E. Koeppe, II. 1992. Molecular determinants of channel function. *Physiol. Rev.* 72:S89–S158.

Andersen, O. S., and J. Procopio. 1980. Ion movement through gramicidin A channels. On the importance of the aqueous diffusion resistance, and ion-water interactions. *Acta Physiol. Scand. Suppl.* 481:27–35.

Arseniev, A. S., V. F. Bystrov, T. V. Ivanov, and Y. A. Ovchinnikov. 1985. ^{1}H-NMR study of gramicidin-A transmembrane ion channel. Head-to-head right-handed, single stranded helices. *FEBS Lett.* 186:168–174.

Becker, M. D., D. V. Greathouse, R. E. Koeppe, II, and O. S. Andersen. 1991. Amino acid sequence modulation of gramicidin channel function: effects of tryptophan-to-phenylalanine substitutions on the single-channel conductance and duration. *Biochemistry.* 30:8830–8839.

Becker, M. D., R. E. Koeppe, II, and O. S. Andersen. 1992. Amino acid substitutions and ion channel function. Model-dependent conclusions. (biophysical discussions). *Biophys. J.* 62:25–27.

Beglov, D., and B. Roux. 1994. Finite representation of an infinite bulk system. Solvent boundary potential for computer simulations. *J. Chem. Phys.* 100:9050–9063.

Brooks, B. R., R. E. Bruccoleri, B. D. Olafson, D. J. States, S. Swaminathan, and M. Karplus. 1983. CHARMM: a program for macromolecular energy minimization, and dynamics calculations. *J. Comput. Chem.* 4:187–217.

Brooks, C. L., III, M. Karplus, and B. M. Pettitt. 1988. Proteins. A theoretical perspective of dynamics, structure, and thermodynamics. *In* Advances in Chemical Physics, Vol. 71. I. Prigogine and S. A. Rice, editors. John Wiley and Sons, New York.

Brüschweiler, R. 1992. Normal modes, and NMR order parameters in proteins. *J. Am. Chem. Soc.* 114:5341–5344.

Busath, D., and G. Szabo. 1988. Permeation characteristics of gramicidin conformers. *Biophys. J.* 53:697–707.

Cross, T. A., and S. J. Opella. 1985. Protein structure by solid-state nuclear magnetic resonance. Residues 40 to 45 of bacteriophage fd coat protein. *J. Mol. Biol.* 182:367–381.

Eisenman, G., and R. Horn. 1983. Ionic selectivity revisited: the role of kinetic, and equilibrium processes in ion permeation through channels. *J. Membr. Biol.* 76:197–225.

Eisenman, G., and J. P. Sandblom. 1983. Energy barriers in ionic channels: data for gramicidin A interpreted using a single-file (3B4S″) model having 3 barriers separating 4 sites. *In* Physical Chemistry of Transmembrane Ion Motions. G. Spach, editor. Elsevier/North Holland Biomedical Press, Amsterdam. 329–348.

Ernst, R. R., G. Bodenhausen, and A. Wokaun. 1987. Principle of NMR in One and Two Dimensions. Clarendon Press, Oxford.

Feller, S. E., and R. W. Pastor. 1996. On simulating lipid bilayers with an applied surface tension: periodic boundary conditions and undulations. *Biophys. J.* 71:1350–1355.

Hille, B. 1992. Ionic Channels of Excitable Membranes, 2nd Ed. Sinauer Associates, Sunderland, MA.

Hille, B., and W. Schwarz. 1978. Potassium channels as multi-ion single-file pores. *J. Gen. Physiol.* 72:409–442.

Hu, W., and T. A. Cross. 1995. Tryptophan hydrogen bonding and electric dipole moments: functional roles in the gramicidin channel and implications for membrane proteins. *Biochemistry.* 34:14147–14155.

Jähnig, F. 1996. What is the surface tension of a lipid bilayer membrane? *Biophys. J.* 71:1348–1349.

Jing, N., K. U. Prasad, and D. W. Urry. 1995. The determination of binding constants of micellar-packaged gramicidin A by ^{13}C- and ^{23}Na-NMR. *Biophys. Biochim. Acta.* 1238:1–11.

Jorgensen, W. L., R. W. Impey, J. Chandrasekhar, J. D. Madura, and M. L. Klein. 1983. Comparison of simple potential functions for simulating liquid water. *J. Chem. Phys.* 79:926–935.

Jorgensen, W. L., and D. L. Severance. 1993. Limited effects of polarization for $Cl^-(H_2O)_n$ and $Na^+(H_2O)_n$ clusters. *J. Chem. Phys.* 99: 4233–4235.

Ketchem, R. R., W. Hu, and T. A. Cross. 1993. High-resolution conformation of gramicidin A in lipid bilayer by solid-state NMR. *Science.* 261:1457–1460.

Koeppe, R. E., II, J. A. Killian, and D. V. Greathouse. 1994. Orientations of the tryptophan 9 and 11 side chains of the gramicidin channel based on deuterium nuclear magnetic resonance spectroscopy. *Biophys. J.* 66:14–24.

Kovacs, H., A. E. Mark, J. Johansson, and W. F. van Gunsteren. 1995. The effect of environment on the stability of an integral membrane helix: molecular dynamics simulations of surfactant protein c in chloroform, methanol, and water. *J. Mol. Biol.* 247:808–822.

Kumar, S., D. Bouzida, R. H. Swendsen, P. A. Kollman, and J. M. Rosenberg. 1992. The weighted histogram analysis method for free-energy calculations on biomolecules. I. The method. *J. Comp. Chem.* 13:1011–1021.

Läuger, P. 1973. Ion transport through pores: a rate theory analysis. *Biochim. Biophys. Acta.* 311:423–441.

MacKerell, A. D., Jr., D. Bashford, M. Bellot, R. L. Dunbrack, M. J. Field, S. Fischer, J. Gao, H. Guo, D. Joseph, S. Ha, L. Kuchnir, K. Kuczera, F. T. K. Lau, C. Mattos, S. Michnick, D. T. Nguyen, T. Ngo, B. Prodhom, B. Roux, B. Schlenkrich, J. Smith, R. Stote, J. Straub, J. Wiorkiewicz-Kuczera, and M. Karplus. 1992. Self-consistent parametrization of biomolecules for molecular modeling and condensed phase simulations. *Biophys. J.* 61:A143.

McGill, P., and M. F. Schumaker. 1996. Boundary conditions for single-ion diffusion. *Biophys. J.* 70:A80.

Nicholson, L. K., and T. A. Cross. 1989. The gramicidin cation channel: an experimental determination of the right-handed helix sense and verification of β-type hydrogen bonding. *Biochemistry.* 28:9379–9385.

Olah, G. A., H. W. Huang, W. Liu, and Y. Wu. 1991. Location of ion-binding sites in the gramicidin channel by x-ray diffraction. *J. Mol. Biol.* 218:847–858.

Patey, G. N., and J. P. Valeau. 1975. A Monte Carlo method for obtaining the interionic potential of mean force in ionic solution. *J. Chem. Phys.* 63:2334–2339.

Prosser, R. W., J. H. Davis., F. W. Dahlquist, and M. A. Lindorfer. 1991. ^{2}H nuclear magnetic resonance of the gramicidin a backbone in a phospholipid bilayer. *Biochemistry.* 30:4687–4696.

Roux, B. 1993. Non-additivity in cation-peptide interactions. A molecular dynamics and ab initio study of Na^+ in the gramicidin channel. *Chem. Phys. Lett.* 212:231–240.

Roux, B. 1995. The calculation of the potential of mean force using computer simulations. *Comp. Phys. Comm.* 91:275–282.

Roux, B., and M. Karplus. 1991a. Ion transport in a gramicidin-like channel: structure and thermodynamics. *Biophys. J.* 59:961–981.

Roux, B., and M. Karplus. 1991b. Ion transport in a gramicidin-like channel: dynamics and mobility. *J. Phys. Chem.* 95:4856–4868.

Roux, B., and M. Karplus. 1993. Ion transport in the gramicidin channel: free energy of the solvated right-handed dimer in a model membrane. *J. Am. Chem. Soc.* 115:3250–3262.

Roux, B., and M. Karplus. 1994. Molecular dynamics simulations of the gramicidin channel. *Annu. Rev. Biomol. Struct. Dyn.* 23:731–761.

Roux, B., and M. Karplus. 1995. Potential energy function for cation-peptide interactions: an ab initio study. *J. Comp. Chem.* 16:690–704.

Roux, B., B. Prod'hom, and M. Karplus. 1995. Ion transport in the gramicidin channel: molecular dynamics study of single and double occupancy. *Biophys. J.* 68:876–892.

Ryckaert, J. P., G. Ciccotti, and H. J. C. Berendsen. 1977. Numerical Integration of the cartesian equation of motions of a system with constraints: molecular dynamics of *n*-alkanes. *J. Comp. Chem.* 23: 327–341.

Schlenkrich, M. J., J. Brickmann, A. D. MacKerell, Jr., and M. Karplus. 1996. An empirical potential energy function for phospholipids: criteria for parameters optimization and applications. *In* Biological Membranes: A Molecular Perspective from Computation and Experiment. K. M. Merz and B. Roux, editors. Birkhauser, Boston. 31–81.

Separovic, F., J. Gehrmann, T. Milne, B. A. Cornell, S. Y. Lin, and R. Smith. 1994. Sodium ion binding in the gramicidin a channel: solid-state NMR studies of the tryptophan residues. *Biophys J.* 67:1495–1500.

Smith, R., D. E. Thomas, A. R. Atkins, F. Separovic, and B. A. Cornell. 1990. Solid-state ^{13}C-NMR studies of the effects of sodium ions on the gramicidin a ion channel. *Biochim. Biophys. Acta.* 1026:161–166.

Smith, R., D. E. Thomas, F. Separovic, A. R. Atkins, and B. A. Cornell. 1989. Determination of the structure of a membrane-incorporated ion channel. *Biophys. J.* 56:307–314.

Teng, Q., and T. A. Cross. 1989. The in situ determination of the ^{15}N chemical-shift tensor orientation in a polypeptide. *J. Magn. Res.* 85: 439–447.

Teng, Q., M. Iqbal, and T. A. Cross. 1992. Determination of the ^{13}C chemical shift and ^{14}N electric field gradient tensor orientations with respect to the molecular frame in a polypeptide. *J. Am. Chem. Soc.* 114:5312–5321.

Teng, Q., L. K. Nicholson, and T. A. Cross. 1991. Experimental determination of torsion angles in the polypeptide backbone of the gramicidin A channel by solid-state by nuclear magnetic resonance. *J. Mol. Biol.* 218:607–619.

Tian, F, K. C. Lee, W. Hu, and T. A. Cross. 1996. Monovalent cation transport: lack of structural deformation upon cation binding. *Biochemistry.* 35: 11959–11966.

Urry, D. W., K. U. Prasad, and T. L. Trapane. 1982a. Location of monovalent cation binding sites in the gramicidin channel. *Proc. Natl. Acad. Sci. USA.* 79:390–394.

Urry, D. W., T. L. Trapane, and K. U. Prasad. 1983. Is the gramicidin A transmembrane channel single-stranded or double stranded helix? A simple unequivocal determination. *Science.* 221:1064–1067.

Urry, D. W., J. T. Walker, and T. L. Trapane. 1982b. Ion interactions in (l-^{13}C) D-Val^8 and D-Leu^{14} analogues of gramicidin A, the helix sense of the channel, and location of ion binding sites. *J. Membr. Biol.* 69: 225–231.

Venable, R. M., Y. Zhang, B. J. Hardy, and R. W. Pastor. 1993. Molecular dynamics simulations of a lipid bilayer and of hexadecane: an investigation of membrane fluidity. *Science.* 262:223–226.

Woolf, T. B., V. G. Malkin, O. L. Malkin, D. R. Salahub, and B. Roux. 1995. The backbone ^{15}N chemical shift tensor of the gramicidin channel: a molecular dynamics and density functional study. *Chem. Phys. Lett.* 239:186–194.

Woolf, T. B., and B. Roux. 1994. Molecular dynamics simulation of the gramicidin channel in a phospholipid bilayer. *Proc. Natl. Acad. Sci. USA.* 91:11631–11635.

Woolf, T. B., and B. Roux. 1996. Structure, energetics, and dynamics of lipid-protein interactions: a molecular dynamics study of the gramicidin A channel in a DMPC bilayer. *Protein Struct. Funct. Genet.* 24:92–114.

Woolf, T. B., and B. Roux. 1997. Influence of small perturbations on the conductance of an ion channel. *In* Towards Molecular Biophysics of Ion Channels. M. Sokabe, A. Auerbach, and F. Sigworth, editors. Elsevier Science Press, Amsterdam. (in press).